Scientific Research Publishing

Materials Sciences and Applications, 2024, 15, 155-167
https://www.scirp.org/journal/msa
ISSN Online: 2153-1188
ISSN Print: 2153-117X

Effect of Dopant Concentration on Luminescence Properties of $KCaPO_4$:Sm

Mieradilijiang Muhetaier, Henglei Chen*, Guangwen Feng, Qun Jing, Qi Liu, Zilong Yin

School of Physics and Technology, Xinjiang University, Urumqi, China

Email: 107552100720@stu.xju.edu.cn, chl@xju.edu.cn, 448532515@qq.com, qunjing@xju.edu.cn, 1015575834@qq.com, yinzilong.edu@163.com

How to cite this paper: Muhetaier, M., Chen, H.L., Feng, G.W., Jing, Q., Liu, Q. and Yin, Z.L. (2024) Effect of Dopant Concentration on Luminescence Properties of $KCaPO_4$:Sm. *Materials Sciences and Applications*, **15**, 155-167.
https://doi.org/10.4236/msa.2024.157011

Received: May 16, 2024
Accepted: July 2, 2024
Published: July 5, 2024

Abstract

$KCaPO_4$ doped with different concentrations of Sm was synthesised by a high-temperature solid-state method, and the crystal structure, morphology, TL and OSL properties of Sm-doped $KCaPO_4$ were systematically investigated by X-ray diffraction (XRD), scanning electron microscopy (SEM), thermoluminescence (TL), and optically stimulated luminescence (OSL) techniques. The results show that 0.3 mol% Sm-doped $KCaPO_4$ annealed at 1073 K for 1 h has the highest TL intensity, and thus is expected to be a candidate material for thermoluminescence dosimetry applications.

Keywords

$KCaPO_4$:Sm, TL, OSL, High-Temperature Solid-State Method

1. Introduction

Radiation dosimeters are pivotal for safeguarding public safety and environmental well-being. In medical contexts, precise dosimetry is indispensable for effective radiation therapy, whereas in nuclear industries and environmental surveillance, they serve to monitor and regulate radiation levels, shielding workers and communities from excessive exposure risks [1]-[3]. Technological progress has fueled the quest for dosimeters with heightened sensitivity and dependability, driving research into novel radiation detection materials and technologies [4].

Optically Stimulated Luminescence (OSL) and Thermoluminescence (TL) technologies harness the energy storage capacity of materials upon radiation

exposure [5]. Upon stimulation by light or heat, these materials emit stored energy, generating a detectable light signal. OSL technology excels due to its straightforward reading process and reusability, while TL technology boasts high sensitivity to low radiation doses [6]. These advancements have not only heightened sensitivity and precision in radiation detection but also broadened their utility across diverse domains including medical dosimetry, environmental radiation monitoring, and personal dose tracking [7] [8].

Phosphate materials, renowned for their stellar luminescent properties and chemical stability, hold immense promise in radiation dosimetry [9]. Their luminescent attributes render them prime candidates for TL and OSL dosimetry applications [10]. Ongoing research on phosphate materials aims at amplifying their luminescent efficiency and stability while broadening their responsiveness to diverse radiation types. Substantial strides have been achieved in recent years towards augmenting the luminescent properties of these materials and optimizing their efficacy in dosimetry applications [11] [12].

Rare-earth doped phosphate materials, owing to their distinctive electronic structures and luminescent properties, have emerged as a focal point in radiation dosimeter research. Incorporating rare-earth elements like Europium (Eu), Dysprosium (Dy), and Thulium (Tm) can notably enhance the luminescent intensity and stability of phosphate materials [13]. These doped materials exhibit superior traits in TL and OSL performance, including heightened sensitivity, an extended linear response range, and enhanced environmental stability [14]. Consequently, rare-earth doped phosphate materials are viewed as a promising avenue for developing a new generation of efficient and stable radiation dosimeters [15]-[17]. In our recent study, we observed that the thermal release intensity of $LiMgPO_4$: Dy samples synthesized via the sol-gel method surpassed those synthesized through the high-temperature solid phase method, albeit with little variance in optical release performance [18].

$KCaPO_4$, as a phosphate matrix, garners attention for its commendable chemical stability and appropriate luminescent properties [19]-[22]. Doping with Samarium (Sm) significantly heightens the luminescent performance of $KCaPO_4$, rendering it a promising contender in TL and OSL dosimetry applications. Sm doping not only amplifies the luminescent efficiency of $KCaPO_4$ but also bolsters its responsiveness to environmental radiation, positioning $KCaPO_4$:Sm as a focal point in radiation dosimeter research [23]. The current research status and future trajectories for $KCaPO_4$:Sm suggest its expansive application potential in radiation dosimetry. Its exceptional thermoluminescent and optically stimulated luminescent properties underscore its prospective value in medical dosimetry and environmental radiation monitoring.

This study's significance lies in delivering an initial evaluation of $KCaPO_4$:Sm as a material for radiation dosimetry, furnishing invaluable insights for crafting a new breed of efficient and stable radiation dosimeters. With radiation dosimeter technology evolving continuously, future research will delve deeper into novel

materials and technologies to fulfill heightened performance demands across an expanded array of application scenarios.

2. Materials and Methods

2.1. High-Temperature Solid-State Method

In this study, $KCaPO_4$ doped with varying concentrations of Sm (0.3, 0.5, 0.7, and 0.9 mol%) was synthesized via the high-temperature solid-state method. Stoichiometric amounts of $CaCO_3$ (99.8%), KH_2PO_4 (99.8%), and $SmNO_{\cdot 6}H_2O$ (99.9%) as the dopant (omitted for the synthesis of undoped $KCaPO_4$) were weighed and mixed. The raw materials underwent grinding in an agate mortar for 40 minutes before being placed in an alumina crucible and heated in a box-type resistance furnace at 550˚C for 2.5 hours. Following natural cooling to room temperature, the sample underwent further grinding, followed by heat treatment at 900˚C for 5 hours. Finally, after natural cooling to room temperature and subsequent grinding, a white powder was obtained.

2.2. Methods of Characterization

The crystal structure of the samples was characterized using a German BRUKER D8-ADVANCE advanced X-ray diffractometer (XRD). The instrument operated with Cu Kα radiation (λ = 1.54 Å) at 40 kV and 40 mA, employing a scanning rate of 5˚/min and covering a scanning range of 10 - 80˚.

The morphology and EDX spectra of KCaPO4 doped with 0.3 mol% Sm were examined using the HITACHI SU8010 field-emission scanning electron microscope (SEM).

The ultraviolet-visible diffuse reflectance spectra (UV-Vis DRS) of the samples were recorded using a PerkinElmer Lambda 650 s UV-Vis spectrophotometer. White $BaSiO_4$ powder served as the reference, with the scanning wavelength range set from 200 to 800 nm.

The excitation and emission spectra of the samples were measured using a HITACHI F-4600 fluorescence spectrophotometer. The slit width was set at 5 nm, and the photomultiplier tube voltage was set to 500 V.

Thermoluminescence (TL) glow curves of the samples were recorded using an LTTL-3DS multifunctional defect fluorescence spectrometer. Powder samples of 0.15 g were pressed into the form of discs with a diameter of 9 mm, The samples underwent X-ray irradiation at a cumulative dose. TL measurements were conducted over a temperature range from room temperature to approximately 800K, employing a heating rate of 3 K/s.

The optically stimulated luminescence (OSL) glow curves of the samples were measured using an SL08 type luminescence meter. The samples underwent irradiation with a β-source at a cumulative dose of 1 Gy. The excitation source utilized a blue LED with a wavelength of 470 nm, operating in CW-BOS mode. OSL signals were recorded at room temperature for 300 s, with data points recorded every 0.5 s.

3. Results and Discussion

3.1. XRD

Figure 1(a) depicts the XRD patterns of $KCaPO_4$ doped with varying concentrations of Sm, synthesized using the high-temperature solid-state method. The synthesized $KCaPO_4$:Sm manifests a single-phase hexagonal structure, with the space group P-3 m1 (164). All peak values correspond to the Powder Diffraction Standard card number 33-1002 of the Joint Committee on Powder Diffraction Standards, indicating $KCaPO_4$ as the predominant crystal phase in all samples, with no other crystal phases present. In Figure 1(b), the XRD local magnification reveals a notable peak shift at 32.4˚ outward as the dopant ion Sm increases within the $KCaPO_4$ structure. This shift may stem from differences in ionic radii of the host ions, where the smaller ionic radii of the rare earths induce a reduction in the cell volume, consequently leading to a shift towards higher diffraction angles. Nonetheless, this shift has had minimal impact on sample purity and has not altered the crystal structure.

3.2. Surface Morphology

Figure 2 displays SEM images of $KCaPO_4$:Sm 0.3 mol% powder, revealing a composition comprising hexagonal structures and irregular particles with some agglomeration. The energy dispersive X-ray (EDX) spectroscopy of $KCaPO_4$:Sm 0.3 mol% (Figure 3) confirms the presence of all elements in the composition, namely K, Ca, P, and O, at the appropriate weight ratio. Additionally, the presence of the dopant Sm is evidenced by a corresponding peak in the spectrum.

3.3. UV-Vis DRS

The UV-visible DRS spectra of $KCaPO_4$ measured at different Sm concentrations, as depicted in Figure 4(a), demonstrate a 1.5-fold increase in reflectance in the doped samples, exhibiting distinct broad peaks near 252 nm and 402 nm,

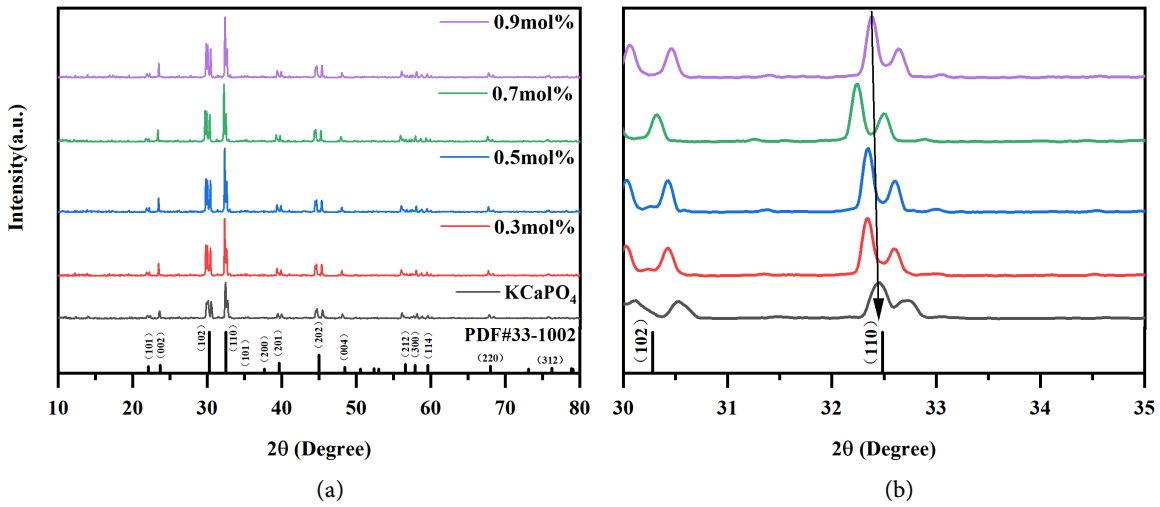

Figure 1. X-ray diffraction patterns of Sm doped polycrystalline $KCaPO_4$ with different dopant concentrations.

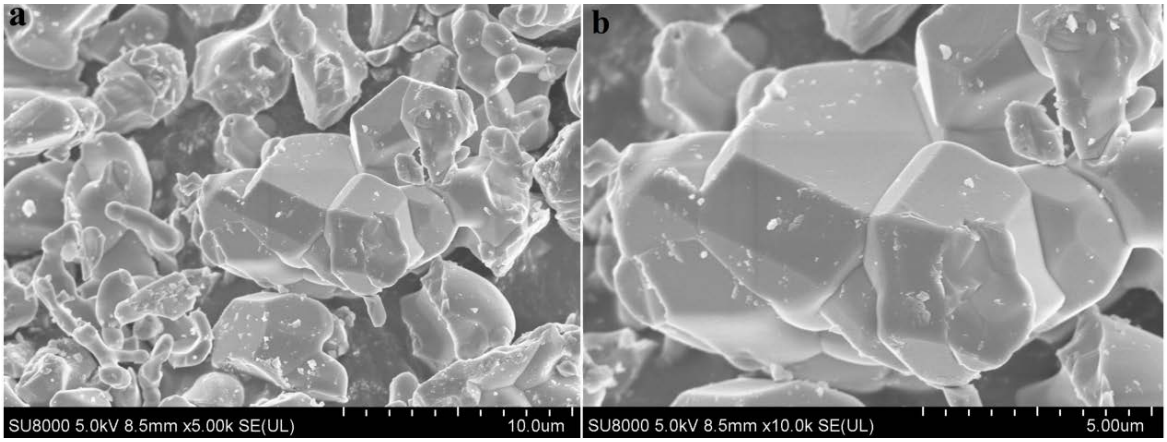

Figure 2. SEM mages of $KCaPO_4$:Sm0.3mol%.

Element	Weight(%)
K	16.53
Ca	16.29
P	15.14
O	51.66
Sm	0.38
Totals	100

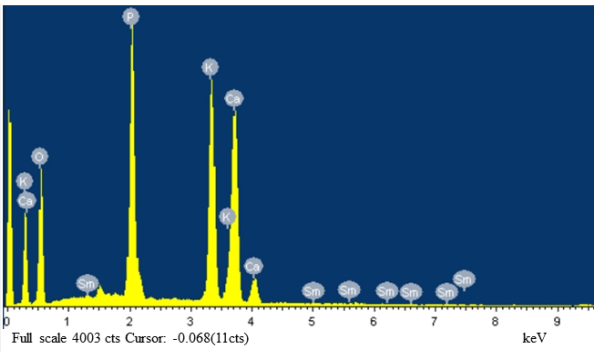

Figure 3. EDX spectrum of $KCaPO_4$:Sm0.3mol% and the amount of concentrations in relation to weight% of different elements present in the samples.

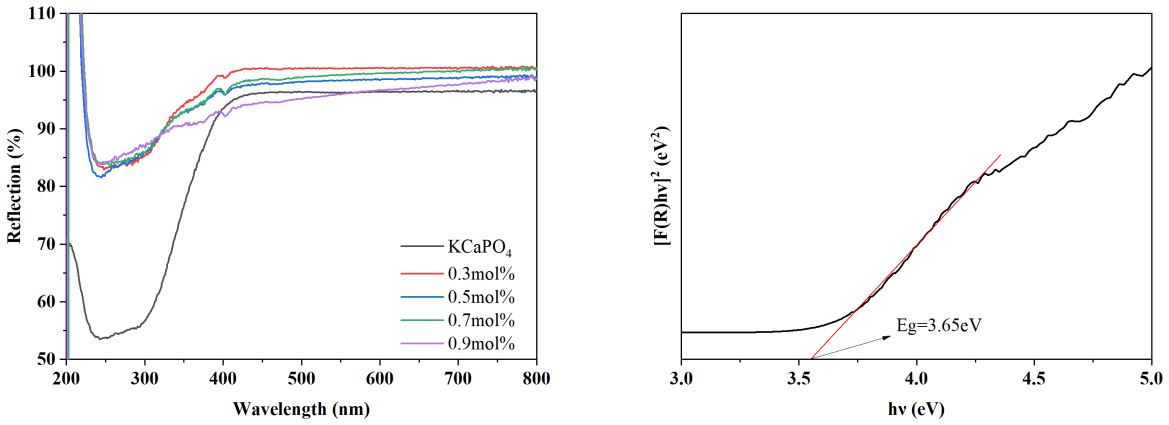

(a) (b)

Figure 4. (a) UV-Vis DRS spectra of $KCaPO_4$ with different concentrations of dopant Sm; (b) curve of $[F(R)h\upsilon]^2$ vs. $h\upsilon$ of $KCaPO_4$.

indicative of interband transitions [24]. A minor blue shift within this broad peak was noted as the doping concentration varied. **Figure 4(b)** illustrates the conversion of undoped $KCaPO_4$ UV-visible DRS spectral data into a pseudo-absorption spectrum F(R) using the Kubelka-Munk function, followed by es-

timating the optical bandgap of the sample using the Tauc formula [25]. The relationship between $[F(R)h\upsilon]^2$ and the photon energy hυ unveiled an optical bandgap value of 3.65 eV for $KCaPO_4$.

3.4. Photoluminescence (PL)

Figure 5 displays the excitation and emission spectra of $KCaPO_4$ at different dopant Sm concentrations. The excitation spectrum of $KCaPO_4$:Sm reveals multiple excitation bands, with the strongest emission peak observed at 402 nm, attributed to the $^6H_{5/2} \rightarrow {}^4F_{7/2}$ transition of Sm (corresponding to the peak at 402 nm in the UV-Vis DRS spectrum) [26]. Upon excitation at 402 nm, the emission spectra of $KCaPO_4$:Sm exhibit peaks at 568 nm, 602 nm, and 650 nm, with the most prominent peak occurring at 602 nm. These peaks correspond to the $^4G_{5/2} \rightarrow {}^6H_{J/2}$ (J = 5, 7, 9) transitions of Sm [27]. The presence of Sm in the main material is evidenced by these sharp peaks.

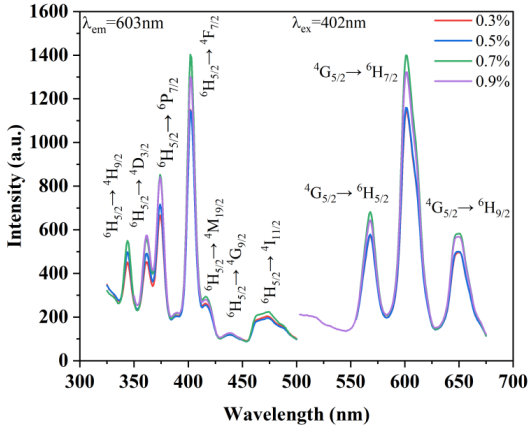

Figure 5. Excitation spectrum and emission spectrum of $KCaPO_4$ with different concentrations of dopant Sm.

3.5. TL Curves of $KCaPO_4$:Sm

The effect of annealing temperature. The effect of annealing temperature on TL was investigated, with TL measurements depicted in Figure 6(a). After cumulative irradiation with X-rays of 10 Gy, It's evident from the figure that the material demonstrates maximum TL intensity in the sample annealed at 1073 K. Conversely, in Figure 6(b), the TL intensity diminishes at 1173 K. The diffusion of ambient oxygen at high temperatures may be the main reason for quenching during high-temperature annealing [28].

Effect of annealing time. The effect of annealing time on TL was investigated, with TL measurements depicted in Figure 7(a). After cumulative irradiation with X-rays of 10 Gy, As shown in the figure, the material demonstrates maximum TL intensity in the sample after annealing for 1 hour. Conversely, in Figure 7(b), the TL intensity decreases after 1.5 hours. The diffusion of ambient oxygen at high temperatures may be the main reason for quenching during high-temperature annealing.

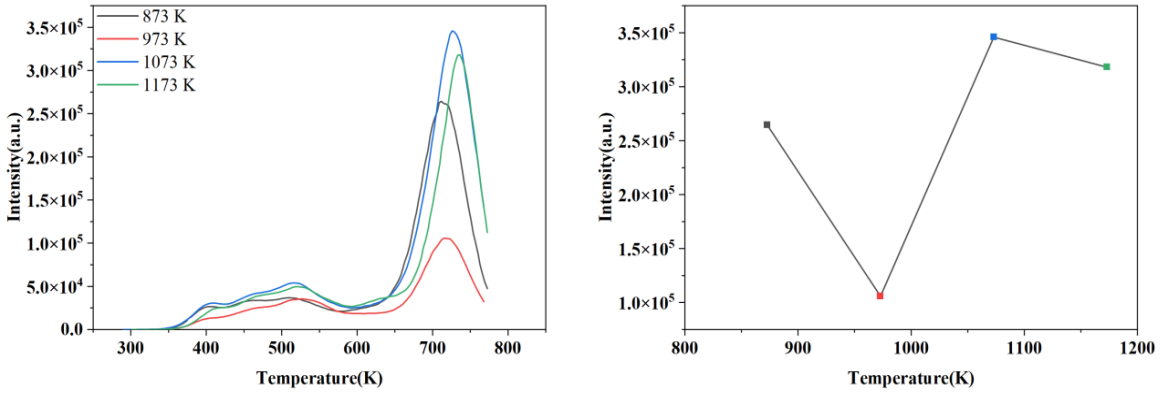

(a) (b)

Figure 6. (a) TL curves of KCaPO4 with different annealing temperatures; (b) Relationship between annealing temperature and TL peak intensity for $KCaPO_4$:Sm.

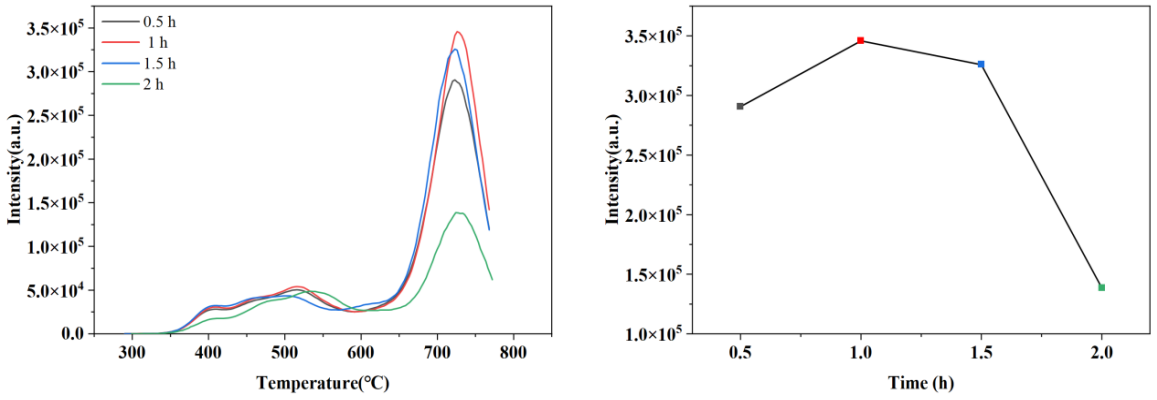

(a) (b)

Figure 7. (a) TL curves of $KCaPO_4$ with different annealing times; (b) Relationship between annealing time and TL peak intensity for $KCaPO_4$:Sm.

Effect of doping concentration on TL. Figure 8(a) illustrates the thermoluminescence glow curves of $KCaPO_4$ doped with varying concentrations of Sm. After cumulative irradiation with X-rays of 10 Gy, Within the 0 to 500˚C range, the undoped sample exhibits three luminescence peaks, with the most intense peak at 144.88˚C, and additional peaks at 213.94˚C and 418.69˚C. Conversely, $KCaPO_4$ doped with different concentrations of Sm (0.3, 0.5, 0.7, and 0.9 mol%) predominantly displays a single luminescence peak, located in the 350-450˚C range, with peak temperatures at 423.44˚C, 408.4˚C, 419˚C, and 413.88˚C, respectively. Sm doping induces alterations in the thermoluminescence intensity of $KCaPO_4$ in the high-temperature region, accompanied by a general shift of low-temperature peak positions towards the high-temperature region. Notably, the pyrorelease intensity in the high-temperature area increases by 2.4 times after Sm doping. Figure 8(b) illustrates how the TL peak intensities of these samples vary with dopant concentrations, highlighting that the sample with a dopant concentration of 0.3 mol% exhibits maximum TL peak intensity.

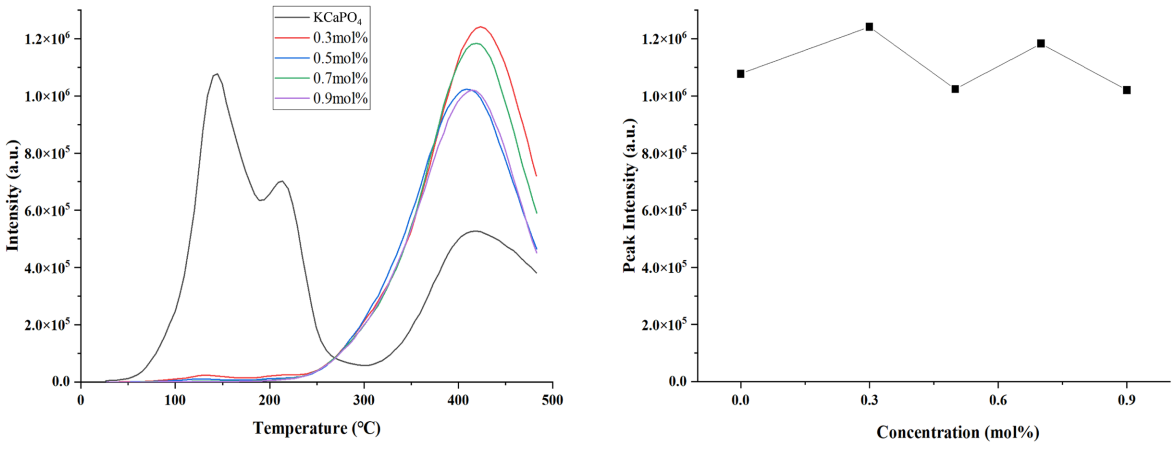

(a) (b)

Figure 8. (a) TL curves of $KCaPO_4$ with different concentrations of dopant Sm; (b) Dopant concentration of $KCaPO_4$:Sm in terms of the TL peak intensity.

Figure 9 presents a comparison of the TL curves under 10 Gy X-ray irradiation between $KCaPO_4$:Sm doped with a concentration of 0.3 mol% and the standard sample (Al_2O_3:C). The sample exhibits maximum TL intensity around 730 K, within a broad emission peak spanning approximately 650 K to 750 K. This broad emission peak is attributed to the continuous distribution of electron traps within the material bandgap. Such traps within the lattice arise from defects naturally occurring during material formation or intentionally introduced by doping with the rare earth element Sm.

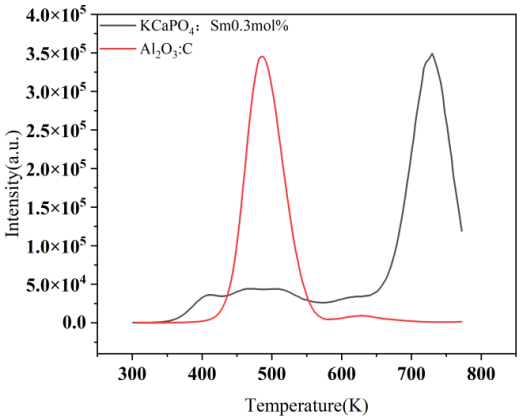

Figure 9. Comparison between TL glow curves of $KCaPO_4$:Sm0.3 mol% and Al_2O_3:C irradiated by 10 Gy dose of gamma rays.

The position, shape, and intensity of the thermoluminescence glow curve reflect the characteristics of the material's energy level traps [29]. Hence, by analyzing the thermoluminescence glow curve, various kinetic parameters can be estimated, including trap depth E, frequency factor s, kinetic order b, and release time t. A Gaussian fit was applied to the thermoluminescence glow curve of the 0.3 mol% Sm-doped sample, as depicted in **Figure 10**. Using Chen's empirical

formula along with the peak shape method, the kinetic parameters of the fitted curve were estimated, including the peak temperature Tm and the half-maximum temperatures on the lower temperature side T_1 and on the higher temperature side T_2. Firstly the geometrical factor denoted by μ_g is [30]:

$$\mu_g = (T_2 - T_m)/(T_2 - T_1) \tag{1}$$

The trap depth E was calculated using Equation (2)

$$E = E_\tau + E_\delta + E_\omega/3 \tag{2}$$

$$E_\sigma = c_\sigma\left(kT_m^2/\sigma\right) - b_\sigma 2kT_m \tag{3}$$

$$\sigma = \tau, \delta, \omega$$

$$c_\tau = 1.51 + 3.0\left(\mu_g - 0.42\right) \tag{4}$$

$$c_\delta = 0.976 + 7.3\left(\mu_g - 0.42\right) \tag{5}$$

$$c_\omega = 2.52 + 10.2\left(\mu_g - 0.42\right) \tag{6}$$

$$\tau = T_m - T_1;\ \delta = T_2 - T_m;\ \omega = T_2 - T_1$$

$$b_\tau = 1.58 + 4.2\left(\mu_g - 0.42\right)$$

$$b_\delta = 0; b_\omega = 1$$

$$\Delta = 2kT_m/E \tag{7}$$

$$\beta E/kT_m^2 = se^{(E/kT_m)}\left[1 + \Delta(b-1)\right] \tag{8}$$

The resulting kinetic parameters are presented in **Table 1**. The frequency factor indicates the number of attempts per second made by trapped electrons to escape the trap, which, in conjunction with temperature and trap depth, determines the stability of the trap. The release time suggests a relatively long average lifetime for the trap. Smaller frequency factor values and longer mean lifetimes of larger traps indicate increased trap stability [31]. With a kinetic order of 1.5, the thermoluminescence glow curve of the sample primarily follows a first-order kinetic equation.

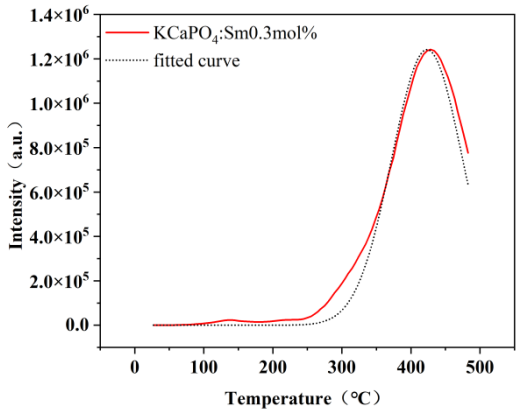

Figure 10. TL deconvolution curve of $KCaPO_4$:Sm0.3mol%.

Table 1. Kinetic parameter values for the $KCaPO_4$:Sm0.3mol% deconvoluted peak.

Peak	T_m (˚C)	μ_g	E (eV)	S (Hz)	t (s)	b
1	418.69	0.48	1.02	2.7×10^{-6}	9.43	1.5

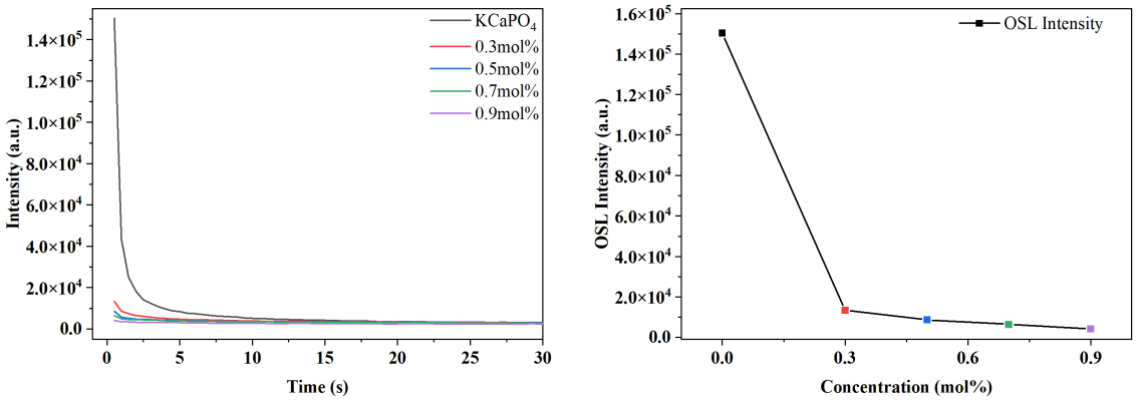

(a) (b)

Figure 11. (a) OSL curves of $KCaPO_4$ with different concentrations of dopant Sm; (b) Dopant concentration of $KCaPO_4$:Sm in terms of the OSL peak intensity.

3.6. OSL Curves of $KCaPO_4$:Sm

Figure 11(a) presents the Optically Stimulated Luminescence (OSL) curves of $KCaPO_4$ doped with different concentrations of Sm. The results indicate that the OSL intensity of the pure sample is stronger than that of the doped samples, and as shown in the inset, the decay rate of the pure sample is slower. **Figure 11(b)** illustrates the relationship between the luminescence intensity in the first second and the doping concentration, revealing a decrease in OSL intensity with increasing doping concentration [28]. This decrease in intensity could be attributed to concentration-quenching effects. The OSL intensity of the pure sample is 150 times greater than that of the doped samples.

4. Conclusion

In this study, different concentrations of Sm-doped $KCaPO_4$ samples were successfully synthesized by the high-temperature solid-state method, and the luminescence properties of the samples were comprehensively compared under different doping concentrations and annealing conditions. XRD patterns showed that the crystal structure remained unchanged with the introduction of the rare earth elements, confirming that all the samples retained the $KCaPO_4$ phase. Scanning electron microscopy images of 0.3 mol% Sm-doped $KCaPO_4$ revealed a combination of hexagonal structure and irregular particles with some agglomerations. EDX spectra confirmed the proper weight ratio of K, Ca, P, O, and Sm, indicating the successful doping of Sm into the crystal lattice. Thermal thermoluminescence curve analysis demonstrated that Sm doping significantly altered the thermoluminescence intensity in the high-temperature region. The thermoluminescence intensity of 0.3 mol% Sm-doped $KCaPO_4$ increased by 2.4 times in

the high-temperature region compared to the undoped sample. Deconvolution of the peaks' dynamic parameters revealed a smaller frequency factor and a larger average trap lifetime, indicating enhanced stability of the traps. Consequently, the material is predominantly controlled by a first-order kinetic equation. Comparison of the optically stimulated luminescence curves for different Sm doping concentrations showed that undoped $KCaPO_4$ exhibited excellent optically stimulated luminescence performance, while luminescent performance weakened after Sm doping. In summary, 0.3 mol% Sm-doped $KCaPO_4$ demonstrated outstanding thermoluminescent properties and holds promise as a candidate material for thermoluminescent dosimetry applications.

Acknowledgments

This work was supported by the Natural Science Foundation of Xinjiang Uygur Autonomous Region (2022D01C51), the National Natural Science Foundation of China (Grants Nos.11864040, 12264047) and the Tianshan Talent Project of Xinjiang Uygur Autonomous Region (2022TSYCJU0004).

Conflicts of Interest

The authors declare no conflicts of interest regarding the publication of this paper.

References

[1] Sahil, Natanasabapathi, G., Shyleshan, S., Kumar, R., Yadav, M.K. and Kumar, P. (2023) Optically Stimulated Luminescence in LiF-MgF_2 System and Its Response as Medical Radiation Dosimeter. *Ceramics International*, **49**, 16352-16362. https://doi.org/10.1016/j.ceramint.2023.01.237

[2] Khandaker, M.U., Mat Nawi, S.N., Lam, S.E., Abdul Sani, S.F., Islam, M.A., Islam, M.A., Naseer, K.A., Osman, H. and Bradley, D.A. (2023) Thermoluminescent Characterization and Defect Studies of Graphite-Rich Media under High Dose Neutron Exposure. *Applied Radiation and Isotopes*, **196**, Article 110771. https://doi.org/10.1016/j.apradiso.2023.110771

[3] Sun, Y., Zhang, S.Y., Shen, G.H., Lin, Q., Chang, Z., Tian, C., Tao, J., Zhang, H., Ding, J., Yuan, B. and Zhang, B. (2023) Radiation Dosimeter and Charge Detector Onboard BeiDou Navigation Satellites in MEO. *Baltic Astronomy*, **32**, Article ID: 2057. https://doi.org/10.1515/astro-2022-0205

[4] Nanto, H. and Okada, G. (2022) Optically Stimulated Luminescence Dosimeters: Principles, Phosphors and Applications. *Japanese Journal of Applied Physics*, **62**, Article 010505. https://doi.org/10.35848/1347-4065/ac9106

[5] Özdemir, A., Can, N., Kurt, K. and Yeğingil, Z. (2018) Optically Stimulated Luminescence (OSL) Dosimetric Properties of $Li_2B_4O_7$: Ag, Gd and Its Relationship with Thermoluminescence (TL) Glow-Curves. *Journal of Alloys and Compounds*, **751**, 159-169. https://doi.org/10.1016/j.jallcom.2018.04.078

[6] Mishra, D.R., Soni, A., Rawat, N.S. and Bokam, G. (2016) Study of Thermoluminescence (TL) and Optically Stimulated Luminescence (OSL) from α-Keratin Protein Found in Human Hairs and Nails: Potential Use in Radiation Dosimetry. *Radiation and Environmental Biophysics*, **55**, 255-264.

https://doi.org/10.1007/s00411-016-0634-9

[7] Chen, R. (2001) IRPA Regional Congress on Radiation Protection.

[8] Ajay Kumar, B. and Hima Bindu, P. (2022) Advances in Borate- and Phosphate-Based TL Materials for *in Vivo* Dosimetry. *Journal of the Korean Ceramic Society,* **59**, 537-550. https://doi.org/10.1007/s43207-022-00240-x

[9] Abdou, N.Y., Farag, M.M. and Abd-Allah, W.M. (2020) Thermoluminescent Properties of Nano-Magnesium Phosphate Ceramic for Radiation Dosimetry. *The European Physical Journal Plus*, **135**, Article No. 317. https://doi.org/10.1140/epjp/s13360-020-00310-1

[10] Mhatre, Sathian, V., Chaudhury, P., *et al*. (2022) Development of Fluorescein-Based Dosimeter for Radiation Processing Applications. *Radiation Protection and Environment*, **45**, 41-47. https://doi.org/10.4103/rpe.rpe_43_21

[11] Huerta, E.F., Soriano-Romero, O., Meza-Rocha, A.N., Bordignon, S., Speghini, A. and Caldiño, U. (2020) Lithium-Aluminum-Zinc Phosphate Glasses Activated with Sm^{3+}, Sm^{3+}/Eu^{3+} and Sm^{3+}/Tb^{3+} for Reddish-Orange and White Light Generation. *Journal of Alloys and Compounds*, **846**, Article 156332. https://doi.org/10.1016/j.jallcom.2020.156332

[12] Chicilo, F., Okada, G., Belev, G., Chapman, D., Edgar, A., Curry, R.J. and Kasap, S.O. (2019) Instrumentation for High-Dose, High-Resolution Dosimetry for Microbeam Radiation Therapy Using Samarium-Doped Fluoroaluminate and Fluorophosphate Glass Plates. *Measurement Science and Technology*, **31**, Article 015201.

[13] Nandanwar, C.M., Kokode, N.S., Yerpude, A.N. and Dhoble, S.J. (2023) Luminescence Properties of $BiPO_4$:Ln (Ln = Dy^{3+}, Tb^{3+} and Sm^{3+}) Orthophosphate Phosphors for Near-UV-Based Solid-State Lighting. *Bulletin of Materials Science*, **46**, Article No. 51. https://doi.org/10.1007/s12034-023-02900-y

[14] Zhu, W., Yang, A., Hao, Z., Cai, C., Wei, J. and Zhang, Y. (2024) Luminous Properties of Highly Moisture-Resistant Dy^{3+}-Tm^{3+}-Eu^{3+} Co-Doped Phosphate Glasses for W-LED. *Ceramics International*, **50**, 3101-3109. https://doi.org/10.1016/j.ceramint.2023.11.057

[15] Jingyuan, G., Chenxi, J., Caixing, Z., Zhengye, X., Luyan, W. and Dongcui, Z. (2023) Dosimetric and Spectroscopic Study of $LiMgPO_4$ Doped with Tm^{3+} and Er^{3+}. *RSC Advances*, **13**, 4949-4957. https://doi.org/10.1039/D2RA07109F

[16] Kellerman, D.G., Kalinkin, M.O., Abashev, R.M., Medvedeva, N.I., Surdo, A.I. and Tyutyunnik, A.P. (2020) Unusual Intrinsic Thermoluminescence in $LiMgPO_4$:Er. *Physical Chemistry Chemical Physics*, **22**, 27632-27644. https://doi.org/10.1039/D0CP05185C

[17] Sas-Bieniarz, A., Marczewska, B., Kłosowski, M., Bilski, P. and Gieszczyk, W. (2020) TL, OSL and RL Emission Spectra of RE-Doped $LiMgPO_4$ Crystals. *Journal of Luminescence*, **218**, Article 116839. https://doi.org/10.1016/j.jlumin.2019.116839

[18] Yin, Z., Chen, H., Feng, G., Jing, Q. and Muhetaier, M. (2023) Study on the Thermoluminescence and Optically Stimulated Luminescence of $LiMgPO_4$: Dy Phosphors Synthesized by Different Methods. *Applied Radiation and Isotopes*, **201**, Article 110990. https://doi.org/10.1016/j.apradiso.2023.110990

[19] Nandanwar, C.M., Kokode, N.S., Nande, A.V., Mungmode, C.D., Yerpude, A.N., Yerojwar, R.M. and Dhoble, S.J. (2023) Photoluminescence Investigation of Novel $KCaPO_4$:Sm^{3+} Phosphors for N-UV Based Solid State Lighting Prepared by Wet Chemical Synthesis. *Optical and Quantum Electronics*, **55**, Article No. 1173. https://doi.org/10.1007/s11082-023-05318-2

[20] Shiratori, D., Kato, T., Nakauchi, D., Kawaguchi, N. and Yanagida, T. (2021) Lumi-

nescence Properties of Eu:$KCaPO_4$ Ceramics That Generate New Luminescent Centers upon X-Ray Irradiation. *Sensors and Materials*, **33**, 2171-2178. https://doi.org/10.18494/SAM.2021.3317

[21] Malik, C., Meena, R.K., Rathi, P., Singh, B. and Pandey, A. (2020) Effect of Dopant Concentration on Luminescence Properties of a Phosphor $KCaPO_4$: Dy. *Radiation Physics and Chemistry*, **168**, Article 108561. https://doi.org/10.1016/j.radphyschem.2019.108561

[22] Palan, C.B. and Omanwar, S.K. (2016) A Novel TL/OSL $MCaPO_4$:Ce (M = Li, K) Phosphor for Radiation Dosimetry. *Optik*, **127**, 7137-7142. https://doi.org/10.1016/j.ijleo.2016.04.117

[23] Fang, H., Huang, S., Wei, X., Duan, C., Yin, M. and Chen, Y. (2015) Synthesis and Luminescence Properties of $KCaPO_4$:Eu^{2+} ,Tb^{3+} ,Mn^{2+} for White-Light-Emitting Diodes (WLED). *Journal of Rare Earths*, **33**, 825-829. https://doi.org/10.1016/S1002-0721(14)60491-9

[24] Noto, L.L., Chitambo, M.L., Ntwaeaborwa, O.M. and Swart, H.C. (2013) Photoluminescence and Thermoluminescence Properties of Pr^{3+} Doped $ZnTa_2O_6$ Phosphor. *Powder Technology*, **247**, 147-150. https://doi.org/10.1016/j.powtec.2013.07.012

[25] Kellerman, D.G., Medvedeva, N.I., Kalinkin, M.O., Syurdo, A.I. and Zubkov, V.G. (2018) Theoretical and Experimental Evidences of Defects in $LiMgPO_4$. *Journal of Alloys and Compounds*, **766**, 626-636. https://doi.org/10.1016/j.jallcom.2018.06.328

[26] Li, G., Chen, W., Wang, Y. and Duhan, B. (2018) Electronic Structure, Photoluminescence and Phosphorescence Properties in Sr_2ScGaO_5:Sm^{3+}. *Dyes and Pigments*, **157**, 259-266. https://doi.org/10.1016/j.dyepig.2018.04.063

[27] Singh, S. (2021) Enhancement and Luminescence Properties of Eu^{3+}, Sm^{3+} co-Doped $KMgPO_4$ Phosphor with Variable Concentration of Eu^{3+} for w-LEDs. *Bulletin of Materials Science*, **44**, Article No. 22. https://doi.org/10.1007/s12034-020-02314-0

[28] Nakata, R., Kohno, K., Sumita, M. and Higuchi, E. (1974) Studies of a New ESR Center in X-Irradiated CaF_2 Crystals. *Journal of the Physical Society of Japan*, **36**, 196-201. https://doi.org/10.1143/JPSJ.36.196

[29] Kalita, J.M. and Chithambo, M.L. (2024) Probing the Electron Trap-Depth Distribution in $Sr_4Al_{14}O_{25}$:Eu^{2+},Dy^{3+}. *Journal of Luminescence*, **265**, Article 120245. https://doi.org/10.1016/j.jlumin.2023.120245

[30] Chen, R. (1969) Glow Curves with General Order Kinetics. *Journal of the Electrochemical Society*, **116**, Article 1254. https://doi.org/10.1149/1.2412291

[31] Chiu, K.P. (2023) The Influence of a Trap State on the Photoluminescence Decay Times under Single Pulse Excitation. *Optical and Quantum Electronics*, **55**, Article No. 163. https://doi.org/10.1007/s11082-022-04433-w